Topics in Catalysis (2023) 66:1381–1390
https://doi.org/10.1007/s11244-022-01778-0

ORIGINAL PAPER

Phosphorus Deactivation on Co-based Catalysts for Fischer-Tropsch

Oscar Ivanez[1] · Anette S. Groven[1] · Kumar R. Rout[1,2] · Edd A. Blekkan[1]

Accepted: 20 December 2022 / Published online: 12 January 2023
© The Author(s) 2022

Abstract
The effect of phosphorus on a cobalt-based catalyst for Fischer-Tropsch Synthesis (FTS) has been investigated. Phosphorus is an impurity present in biomass and, in this work, its deposition on the catalyst during biomass to liquid (BTL) operation, based on gasification and FTS, has been mimicked. For this purpose, four different cobalt-manganese-rhenium catalysts supported on alumina were prepared by incipient wetness impregnation with different phosphorus loadings. The results showed that below 800 ppm of phosphorus, the catalysts performance was not significantly affected, possibly because the interaction of phosphorus mainly was with the alumina support. However, above this threshold, the effect of phosphorus was noticeable with a decrease in intrinsic activity. The reduced performance can be attributed to a physical blocking of cobalt sites. But, in all poisoned catalysts, the product distribution was affected and shifted towards less valuable products as methane and light paraffins. The electronegativity of phosphorus might be the cause for this effect, as the effective H_2/CO ratio on the catalyst surface may be increased due to a weakened metal-CO bonding and consequently, the selectivity of the hydrogenated products increased.

Keywords Fischer-Tropsch · Cobalt oxide · Biomass to liquids · Phosphorus · Deactivation

1 Introduction

The exponential growth of the global industry demands improvement and development of new technologies for the production of fuels and chemicals. The main source of energy is fossil fuels, and their use has steadily increased over the decades. In 2020, more than 80% of the primary energy in the world was provided by fossil fuels. However, in light of climate change, international agreements and increased prices of fossil fuels, the demand for clean and sustainable fuels is rapidly rising, requiring alternative fuel and chemicals production [1]. In this context, biomass has the potential to be a source for hydrocarbon products, due to feedstock flexibility and the possibility to reduce net CO_2 emissions by using sustainable sources of carbon. One of the processes to valorize biomass is via biomass to liquids (BTL), in which the biomass is transformed to synthesis gas and subsequently to liquid fuels.

Synthesis gas can be converted to chemicals or fuels via a range of different processes. An interesting alternative is Fischer-Tropsch synthesis (FTS), a catalytic reaction by which syngas is transformed into a wide range of hydrocarbons. The reaction can be catalyzed by group VIII elements, but in commercial applications only Fe and Co are currently employed. Cobalt is interesting due to its high activity at low temperature (200 – 300 ºC), high selectivity towards long chain hydrocarbons, low production of oxygenates and alkenes and high durability. However, by optimizing the synthesis method and operation conditions, it is possible to tune the selectivity towards different products. To increase the profitability of the BTL and FT process, it is possible to adjust the product distribution to more valuable products. Among the FT products, light olefins represent added value compared to fuels, which always will be the main product [2]. The demand for these products has been increasing every year. Ethylene, propylene and olefinic C_4 fractions, mostly produced by steam cracking or recovered from oil refineries, are key building blocks in the petrochemical industry. In the case of propylene, the gap between the

✉ Oscar Ivanez
Oscar.l.i.encinas@ntnu.no

1 Department of Chemical Engineering, Norwegian University of Science and Technology (NTNU), Sem Saelands vei 4, 7491 Trondheim, Norway

2 SINTEF Industry, P.O. Box 4760, NO-7465 Torgarden, Trondheim, Norway

demand and the capability of production has been broadening since 2011 [3]. This scenario opens the possibility for new and renewable processes for the production of these products. FTS to olefins, also called FTO, has the potential of reducing the overall cost by the direct production of light olefins without intermediate steps [4][5]. Translated to operation conditions, a higher temperature, lower pressure, and a hydrogen deficient syngas would increase the product distribution towards these chemicals [6]. Furthermore, the addition of the right promoters to the cobalt catalysts can also improve the selectivity towards light olefins. Rhenium has been studied widely as a promoter for the FT cobalt catalysts due to the improvement in reducibility and metallic dispersion of the catalyst by hydrogen spillover [7]. Manganese promotion has been also studied due to its influence shifting the product distribution to lighter olefins and decreasing methane selectivity [8], as well as increasing the intrinsic activity of the catalyst [9].

The use of biomass as source of syngas has its own advantages and drawbacks. On one hand, this renewable energy source is abundant and opens the possibility to improve the total yield of different industries by using waste as a feedstock for the BTL. As an example, the total fish production in Norway in 2019 was 2.309.319 tons, with 68% of the amount being edible [10]. The waste formed, including the sludge, is rich in carbon and represents an opportunity for valorization by gasification in order to reduce the economic losses and improve the efficiency of the industry [11], [12]. Forest residues represent another sustainable source of carbon that can be utilized this way [13]. On the other hand, BTL is a difficult process. It is characterized by several steps, consisting of the reception and handling of biomass, the biomass gasification to produce synthesis gas, the syngas cleaning and adjustment and finally, the hydrocarbon synthesis followed by refining to produce the fuel according to specifications. Gas cleaning is one of the most difficult challenges to overcome in order to make BTL feasible [14]. The syngas composition depends on the type of biomass selected and type of gasifier [15] but it mainly contains H_2 and CO. The biomass is mainly composed by C, O and H, with traces of N and S and a range of other elements. The main contaminants in biomass-based syngas are sulfur (H_2S, COS and organically bound sulfur), ammonia and HCN, condensable hydrocarbons like tars, and ash components, mainly as particulates or in case of high-temperature gasification (entrained flow) also as vapors.

These components must be removed before any catalytic syngas upgrading. Depending on the plant for fuel synthesis process, catalysts, etc. the requirements of the syngas are different. The effect of sulfur, alkali metals and nitrogenated compounds on the FT catalyst has been extensively documented. However, biomass has a wide range of other inorganic species present in the ashes and their effects have not been entirely investigated. The ashes are the non-combusted inorganic species with a particle size ranging from 1 to 100 µm. These components vary in composition, but it is formed mainly by alkali and alkaline earths metals (Na, K, Mg, Ca) and other elements (Ti, Mn, Fe, Al, Si, P, Cl). Most of these inorganic species will end up in different amounts in the gas phase following gasification [16]. For the utilization of the syngas, most of the applications requires a 99% article removal [17]. There are different technologies to remove the contaminants present in the syngas and the degree of removal will set the final operation cost of the whole process. Understanding the acceptable level of contamination in the catalysts can lead to a reduction in the overall cost of the syngas clean-up. In addition, is also interesting to understand the behavior of the catalyst in the reaction due to the contaminants, as the knowledge can improve the BTL technologies. As mentioned before, one major inorganic component of the animal biomass are phosphoric species [17], [18], mostly in form of P_4O_{10} after the gasification, reaching more than 40% the content in the ashes for certain types of biomasses. Some of the P will also be present in the gas phase, with concentrations above 25 ppmw being reported following fluid bed gasification [19]. The effect of phosphorus as a contaminant for further applications of the syngas has not received much attention. There are some studies of phosphorus promotion [20], [21], but the addition has been during the catalyst preparation before the addition of cobalt as a promoter and used to modify the support. The main objective of these studies was to form mixed oxides with the phosphorus and the support, in order to modify the surface of the support to enhance different properties as the metallic dispersion and suppress metal-support interactions [22][23][24]. In this study, we explore the effect of phosphorus deposition on a cobalt-based FT catalyst after the preparation of the catalyst, as an attempt to better mimic the interaction between the phosphorus and the catalyst. Therefore, this study will contribute to the understanding of the deactivation of the active phase that phosphorus could lead to if it is deposited on the catalyst during FTS while using a cobalt-based system promoted by manganese and rhenium to maximize olefin production.

2 Experimental

2.1 Catalyst Preparation

To investigate the effect of phosphorus in the FTS, four different cobalt-manganese-based catalysts supported on γ-alumina were prepared with increased phosphorus content, from 0 ppm to 6700 ppm. The reference catalyst was

loaded with 15 wt% Co, 3.75 wt% Mn and 0.5 wt% Re, supported on γ-alumina (Sasol Puralox SCCa 45/190). The catalyst was prepared by two step incipient wetness impregnation following the work of Pedersen et al. [25]. First, the manganese was deposited in the γ-alumina by means of an aqueous solution of $Mn(NO_3)_2 \cdot 4H_2O$. After the impregnation, the solid was dried in a stationary oven at 383 K for 12 h. The dried catalyst was calcined in air at 573 K (1 K/min) for 10 h. Subsequently, the cobalt and rhenium were added to the solid by a solution containing $Co(NO_3)_2 \cdot 6H_2O$ and $HReO_4$. The drying and heat treatment followed the same procedure mentioned before. To prepare the poisoned catalysts, the phosphorus was added to the reference catalyst by means of incipient wetness impregnation by a water solution of H_3PO_4. The catalysts were dried at 383 K and calcined in air at 573 K (1 K/min) for 4 h. The reference catalyst is named $CoReMn/Al_2O_3$ and the poisoned catalysts 8P – $CoReMn/Al_2O_3$ (800 ppm of P), 17P – $CoReMn/Al_2O_3$ (1700 ppm of P) and 67P – $CoReMn/Al_2O_3$ (6700 ppm of P). Prior to all experiments, the catalysts were sieved to a particle size of 54 – 90 µm.

2.2 X-ray Diffraction

X-ray diffraction (XRD) studies were performed in a Bruker D8 DaVinci X-ray diffractometer instrument with CuKα radiation. The experiments were performed in the calcined catalysts and the crystal size was obtained from the most intense peak by using the Scherrer equation. The cobalt oxide crystal size was corrected to metallic cobalt according to the relative molar volumes resulting in the following Eq. (1) [26]:

$$d = 0.75 \cdot d_{Co_3O_4} \tag{1}$$

Where d is the metallic cobalt crystal size and $d_{Co_3O_4}$ is the cobalt oxide crystal size. The metallic dispersion was calculated by the following Eq. (2) assuming spherical and uniform cobalt particles with a site density of 14.6 atoms/nm^2 [27].

$$D = \frac{96}{d} \tag{2}$$

Where D is the metallic dispersion (%) and d is the cobalt particle size (nm).

2.3 N_2 Volumetric Adsorption

The surface area, average pore size and pore volume measurements were performed in a Tristar 3000 by volumetric nitrogen adsorption-desorption. Before the experiments, the samples (~150 mg) were degassed in vacuum overnight at 200 ºC. For calculating the surface area, the Brunauer-Emmet-Teller (BET) isotherm was used. For the pore volume and average pore size, the Barret-Joyner-Halenda (BJH) method was utilized.

2.4 H_2 Chemisorption

H_2 chemisorption was measured in a Micromeritics Asap 2010 instrument. A quartz U-shaped tubular reactor was loaded with ~200 mg of catalysts and reduced with H_2 at 623 K (1 K/min) for 16 h. After the reduction, the samples were evacuated for 1 h at 603 K and then cooled to 313 K. The adsorption isotherm was measured between 0.01 – 0.67 bar. The volume of chemisorbed hydrogen was obtained by the extrapolation to zero pressure of the linear part of the isotherm. For the calculation of the metallic surface area, it was assumed that only the cobalt contributes to the chemisorption of hydrogen and that one atom of hydrogen bonds to one atom of cobalt.

2.5 Temperature-programmed Reduction

Temperature-programmed reduction (TPR) experiments were carried out in an Altamira-300RHP. The catalyst (~100 mg) was loaded in a U-shaped tubular reactor constructed from quartz and heated to 973 K (10 K/min) in 50 ml/min gas flow consisting of 7% hydrogen in Argon. The temperature was held for 1 h and then the sample was cooled to room temperature. The H_2 consumption was measured by a thermal conductivity detector.

2.6 H_2 Temperature-programmed Desorption

Temperature-programmed desorption (TPD) experiments were carried out in an Altamira-300RHP. The catalyst (~100 mg) was loaded to a quartz U-shaped tubular reactor and reduced with 50 ml/min of H_2 at 623 K (1 K/min) for 16 h. Two different experiments were performed depending on the temperature of the sample. The sample temperature was adjusted to 313 or 483 K and then calibrated pulses of H_2 were added to the sample until no further consumption of H_2 was detected. In both experiments, the sample was then purged for 20 min in helium to remove hydrogen that was not chemisorbed and heated to 973 K (10 K/min) with 50 ml/min of argon. The TPD spectra was measured by a thermal conductivity detector.

2.7 Fischer-Tropsch Synthesis

The Fischer-Tropsch synthesis was performed in a stainless-steel fixed bed reactor (i.d. 10 mm) at 513 K and 5 bar. The

Table 1 Surface properties of the Al_2O_3 and $CoReMn/Al_2O_3$ with increasing phosphorus loading including BET surface area, pore volume and pore size and metallic dispersion (D) and particle size (D_p) by H_2 chemisorption (a) and XRD (b)

Catalyst	BET surface area (m^2/g)	Pore volume (cm^3/g)	Pore size (nm)	D (%) [a]	D_p (nm) [a]	D (%) [b]	D_p (nm) [b]
Al_2O_3	182	0.73	12.4	-	-	-	-
$CoReMn/Al_2O_3$	143	0.49	11.4	7.8	12.3	8.3	11.5
8P-$CoReMn/Al_2O_3$	142	0.49	11.5	7.7	12.5	8.3	11.5
17P-$CoReMn/Al_2O_3$	140	0.49	11.4	6.7	14.2	8.0	12.0
67P-$CoReMn/Al_2O_3$	134	0.49	11.6	6.5	14.6	8.0	12.0

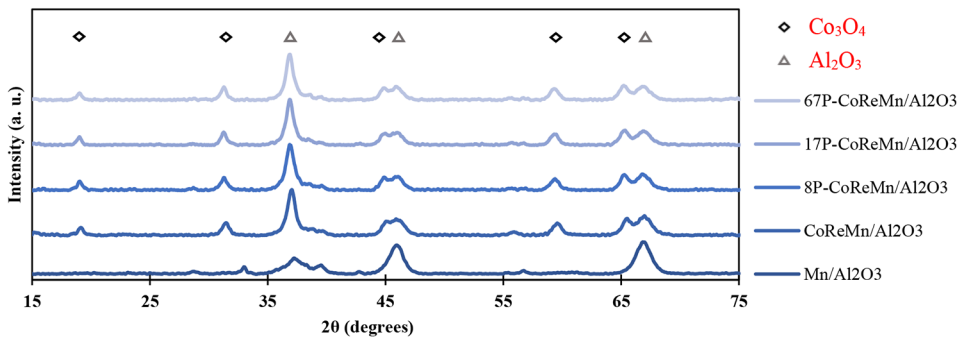

Fig. 1 X-ray diffraction patterns of the Mn/Al_2O_3 and $CoReMn/Al_2O_3$ with increasing phosphorus loading

catalyst (1 g, 54–90 µm) was diluted with of SiC (19 g, 90–250 µm) to improve the heat distribution along the catalyst bed. In addition, to further reduce possible hotspots in the bed, the reactor was placed inside an aluminum block and mounted in an electrical furnace. Before the FTS, the catalyst was activated by the reduction in a flowing mixture of 125 – 125 ml/min of H_2 – He for 10 h at 623 K (1 K/min). After the reduction, the catalyst was cooled down to 443 K and pressurized to 5 bars in Helium flow. For the FTS, 250 ml_N/min of synthesis gas with a H_2:CO ratio of 1.7 and 3% of N_2 as internal standard was introduced to the reactor. The temperature was then increased to 503 K (20 K/min) and, slowly to the reaction temperature of 513 K (5 K/min). The liquid FT products were condensed in a hot trap (~363 K) and a cold trap kept at ambient temperature. The remaining gas products were analyzed using an Agilent 6890 N gas chromatograph equipped with two columns: a Carbosieve with a thermal conductivity detector (TCD) for permanent gases and an Al_2O_3-PLOT with a flame ionization detector (FID) for light hydrocarbons. The activity of the catalyst was compared in terms of CO conversion and Site-Time Yield (STY) (defined as moles CO converted per surface cobalt atom and second) during the first 24 h. To compare the selectivity, the CO conversion was adjusted to 50% by modifying the space velocity. The selectivity is reported in terms of CH_4, C_{2-4} alpha olefins and C_{2-4} paraffins and C_{5+}, based on the assumption that C_1-C_4 hydrocarbons are recovered in the gas-phase following condensation of the liquids.

3 Results and Discussion

3.1 Catalyst Characterization

The elemental bulk composition of the catalysts was studied by means of X-Ray fluorescence, confirming the desired loadings of the different elements (not showed). In Table 1, the main properties of the catalysts, including the results from the N_2 volumetric adsorption, H_2 chemisorption and XRD are summarized.

X-ray diffraction was used to identify the crystalline phases present in the catalysts. The diffractograms are shown in Fig. 1. The manganese oxide signal can be seen at 28, 37, 43 and 56 degrees. However, these reflections are not visible on the catalyst containing cobalt indicating that the manganese might be well dispersed on the support or incorporated into the cobalt oxide lattice. The characteristic cobalt oxide (Co_3O_4) signal is visible at 37 degrees. However, there is no visible signal for phosphorus impeding the identification of any cobalt-phosphorus species. At this resolution, the lower loadings of phosphorus do not seem to have an impact on the cobalt crystallinity. Still, as presented in Table 1, the addition of higher loadings led to a slightly increase in the cobalt crystal size. This suggests that the phosphorus particles are smaller than 3 nm and thus, are not detected by XRD or incorporated into the cobalt oxide lattice.

N_2 volumetric adsorption was used to study the morphological properties of the catalysts. The BET surface area, pore volume and average pore size obtained by the BJH method are shown in Table 1. There is some decrease in

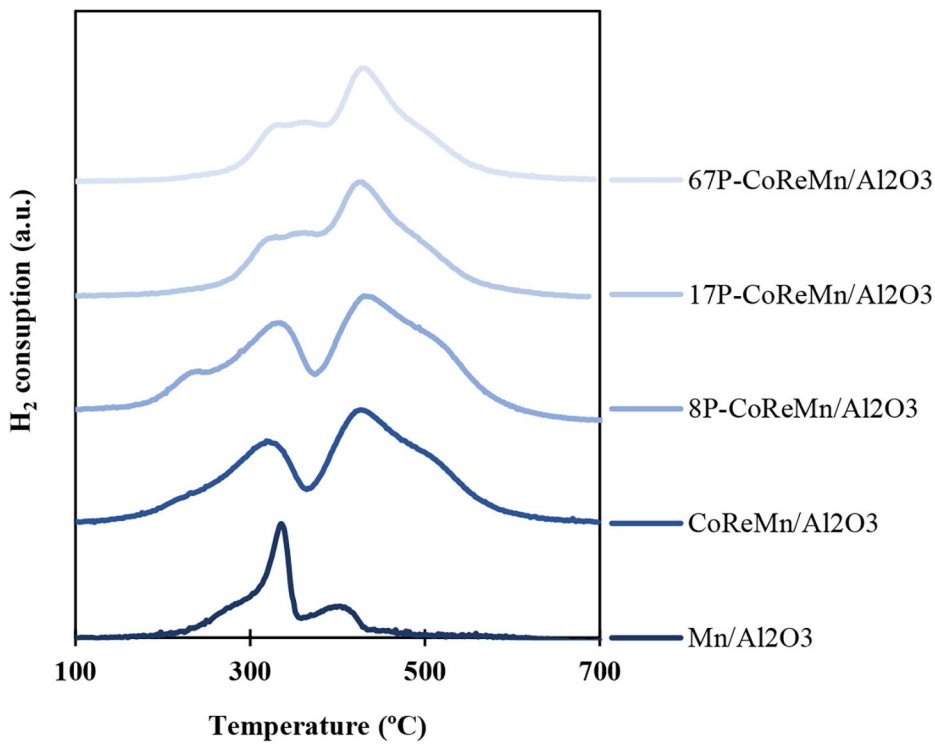

Fig. 2 Temperature-Programmed Reduction profile of the Mn/Al_2O_3 and $CoReMn/Al_2O_3$ with increasing phosphorus loading from 100 ºC to 700 ºC

the surface area, pore volume and pore size with the addition of cobalt to the alumina support. However, the addition of phosphorus to the catalyst did not significantly affect the morphological characteristics, with only a slight reduction in the surface area. This suggests the deposition of highly dispersed phosphorus entities without physically obstructing the pores of the support, and therefore, keeping the cobalt particles accessible.

Similarly, the results for the metallic dispersion and the particle size obtained by hydrogen volumetric chemisorption and by XRD are shown in Table 1. The results revealed a decrease in metallic dispersion from 7.8 to 6.5% based on H_2 chemisorption with increased content of phosphorus. Equally, the calculated particle size increased from 12.3 to 14.6 nm. These particle size values are above the threshold of approximately 6–8 nm which is known to influence the activity of the catalyst [28]. However, based on XRD, the dispersion and particle size remained relatively constant. This disparity in the results suggests that the difference in H_2 consumption per cobalt atom for the reference and poisoned catalysts are not caused by an increase in particle size. The most likely explanation is the blocking of hydrogen chemisorption on the cobalt particles by the phosphorus deposition, already described by other studies [21], [29]. This supports the theory that the phosphorus is deposited on top of the cobalt particles inhibiting the H_2 adsorption and therefore, reducing the measured metallic dispersion.

The temperature-programmed reduction was performed to study the effect of the addition of phosphorus on the reducibility of the catalyst. The TPR profiles are shown in Fig. 2. The first profile corresponds to the reduction of manganese oxide. The catalyst showed one large peak attributed to the reduction of Mn_2O_3 and MnO_2 to Mn_3O_4, at 330 ºC and a smaller peak attributed to the reduction to MnO at 400 ºC [30]. The first shoulder, at around 250 ºC, is attributed to the manganese nitrate precursor residue. The next profile corresponds to the reference catalyst with cobalt rhenium and manganese. The results showed a typical cobalt supported on alumina TPR profile [7], with the reduction from Co_3O_4 to CoO at 320 ºC and then, to metallic cobalt starting at 430 ºC. The addition of 800 ppm of P did not significantly affect the reducibility of the catalysts, with only a small shift of the first peak to slightly higher temperature (330 ºC). This small change can be attributed to the phosphorus interacting mostly with the alumina and not with the cobalt and therefore, not affecting the reducibility of the cobalt particles. However, above 800 ppm, the double peak profile is lost. The profile shows one big shoulder formed by two peaks, one at 330 ºC and the other at 360 ºC. If we compare the poisoned catalysts TPR profiles with the Mn/Al_2O_3 profile, we can see that the peak at 330 ºC, attributed to the manganese reduction, is maintained while the cobalt peak is altered. This shifting towards higher temperatures suggests that phosphorus interacts strongly with Co_3O_4 particles, resulting in a decreased reducibility. It is also possible that

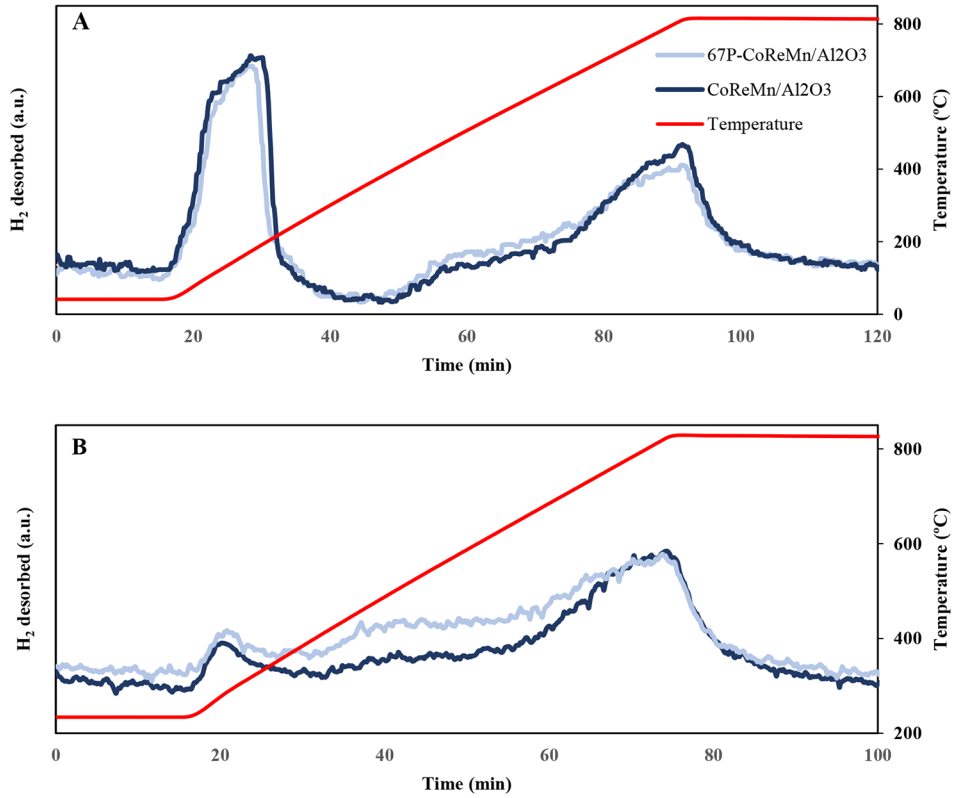

Fig. 3 H_2-TPD with pulses at 40 ºC (A) and 210 ºC (B) of the CoReMn/Al_2O_3 and 67P-CoReMn/Al_2O_3

less reducible cobalt-phosphide species could be formed in P-doped catalysts. With respect to the second peak and with the total hydrogen uptake, there are no significant differences between the poisoned and reference catalysts, suggesting that the reducible fraction of cobalt is not altered by the presence of phosphorus.

A comparison of the H_2-TPD of the catalyst CoReMn/Al_2O_3 and 67P-CoReMn/Al_2O_3 is depicted in Fig. 3. In Fig. 3-A, the experiments in which the pulses were carried out at 40 ºC are represented, while in Fig. 3-B the pulses were performed at 210 ºC. Both H_2-TPD curves follow the same trend consisting of a two-peak profile, with a first peak at 185 ºC and 285 ºC in Fig. <link rid="fig3">3</link>-A and 3-B, respectively, while a second peak was detected in both experiments at a temperature around 815 ºC. No major differences were observed on the amount of H_2 adsorbed during the pulsing or H_2 desorbed during the TPD on the reference and poisoned catalyst. This implies that the phosphorus does not affect the hydrogen desorption in our case, in contrast to the study performed by Martinelli et al. who reported that phosphorus might inhibit the H_2 desorption [21].

3.2 Activity Measurements

The CO conversion over the first 24 h on stream is shown in Fig. 4 – A (the first hours until the CO conversion was stabilized are not shown). The CO conversion slightly decreases for all the catalysts during the first 24 h, yet all of the samples displayed significant stability. The conversion displayed by the 8P-CoReMn/Al_2O_3 and reference catalysts were almost equivalent with no reduction in the activity of the poisoned catalysts. These results are in agreement with the characterization results, and this behavior can be explained by the phosphorus being mostly interacting with the support and not in contact with the active phase, as also indicated by the TPR experiments. However, once the loading of phosphorus increases, there is a notable decrease in conversion. These results are in disagreement with previous studies, where it was found that more than 1% of phosphorus was necessary in order to see significant deactivation [20]. However, the preparation method as well as the support employed in the study was different. In the study performed by Gnanamani et al. SiO_2 support was used and it is possible that the different support-metal interactions as well as the ability and capacity of the support surface to adsorb the P-species on SiO_2 and Al_2O_3, respectively play a role and modify the effect of phosphorus during the reaction. The CO conversions at fixed conditions is reduced from 51% to 40% nd 36% ith the addition of 0.17% nd 0.67% f phosphorus respectively, indicating that there is a threshold in phosphorus loading, above which the performance of the catalyst is affected. However, this effect appears not to be proportional with the P loading, since a reduction in CO

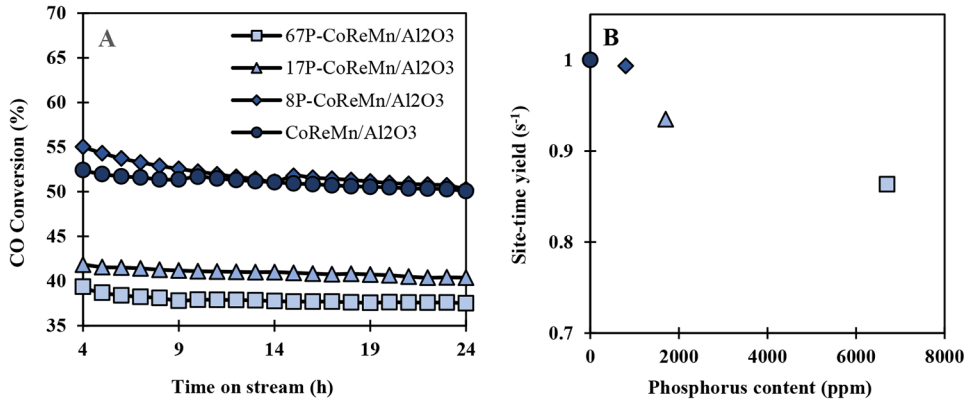

Fig. 4 CO conversion, at 240 ºC, 5 bar and 15 L/gcat*s, during the first 24 (A) h on stream and the Site-Time yield (B) at 24 h on stream conversion of $CoReMn/Al_2O_3$ with increasing phosphorus loading

Table 2 GHSV required to achieve 50% of CO conversion for the different catalysts and selectivity (%) to the different product fractions, from CH_4 to C_{5+}. The paraffinic products are represented by -, while the olefins are represented by =

Catalyst	GHSV (L/g·h)	CH_4	C_{2-}	$C_{2=}$	C_{3-}	$C_{3=}$	C_{4-}	$C_{4=}$	C_{2-4-}	$C_{2-4=}$	C_{5+}
$CoReMn/Al_2O_3$	15.0	13.5	1.9	0.2	1.8	3.9	2.4	2.7	6.1	6.8	70.8
8P-$CoReMn/Al_2O_3$	15.0	14.0	2.0	0.1	2.0	3.7	2.6	2.3	6.6	6.3	70.2
17P-$CoReMn/Al_2O_3$	12.0	16.2	2.1	0.1	2.6	3.6	3.1	2.0	8.1	5.8	66.4
67P-$CoReMn/Al_2O_3$	11.1	17.7	2.6	0.1	3.5	2.8	3.8	1.3	9.4	4.3	64.3

conversion from 51% to 40% 22% eduction) is seen with an addition of 1700 ppm of P, but a further increase of the loading to 6700 ppm only leads to a minor additional reduction of the conversion to 36% 30% eduction).

The normalized STY, based on the H_2 chemisorption, at 24 h on stream is represented in the following Fig. 4 – B. STY depicts the activity per cobalt active site and the same trend is observed as in the CO conversion, with an insignificant effect at the lowest loading and an increased effect with more phosphorus content. Based on previous studies, the STY is independent on the cobalt dispersion and nature of the support [31], therefore the differences in dispersion, based on H_2 chemisorption, should not influence the catalytic activity.

The results indicate a complicated relationship between the amount of P deposited on the catalysts and the decrease in dispersion and activity. This indicates that the effect of P is both due to blocking of cobalt active sites as well as an influence, typically electronic, on the activity. If it is considered that the site blocking due to the P is the only cause for the deactivation, for the 17P – $CoReMn/Al_2O_3$, 1 atom of P would be blocking 3 cobalt sites, while for 67P – $CoReMn/Al_2O_3$, 1 atom of P would be blocking 1.6 cobalt sites. This difference suggests that there are other mechanisms of the deactivation rather than just physical blocking of cobalt particles. The electronegativity of the P might play a role in the deactivation of the catalyst [32]. Previous studies on the effect of promoters based on the Lewis acidity [33] showed that the CO adsorption can be weakened due to electron withdrawal from the cobalt resulting in a lower adsorbed CO/H ratio on the Co surface, leading to a decreased activity.

3.3 Selectivity Measurements

To consistently compare the product distribution, the CO conversion was adjusted to 50%, by means of modifying the space velocity, after the first 24 h on stream. In Table 2, the required space velocity to achieve 50% of CO conversion is described. In addition to the specific selectivity towards methane, C_{5+} products and the light paraffinic and α-olefinic products are reported.

In Fig. 5, the selectivity to C_{5+} products (5 – A), $C_2 - C_4$ α-olefins (5 – B), CH_4 (5 – C) and $C_2 - C_4$ paraffins (5 – D) are shown. As expected with the cobalt-based catalysts, the selectivity to ethylene is very low due to readsorption and further reaction (chain growth). However, the selectivity towards propylene is the highest among the light olefins [34]. On the other hand, the effect of the phosphorus on the selectivity to all product fractions is appreciable, with an increase in methane and light paraffins and a reduction in light α-olefins and chain growth. This effect on the catalyst suggests that there is an increase in the rate of hydrogenation reactions and a reduction in the chain growth probability. This effect is more noticeable with increased phosphorus loading in the catalysts. It is interesting to note that the addition of 800 ppm of phosphorus did not affect the activity of the catalyst, but it did influence the selectivity, suggesting that the mechanism of the influence on activity and selectivity is different.

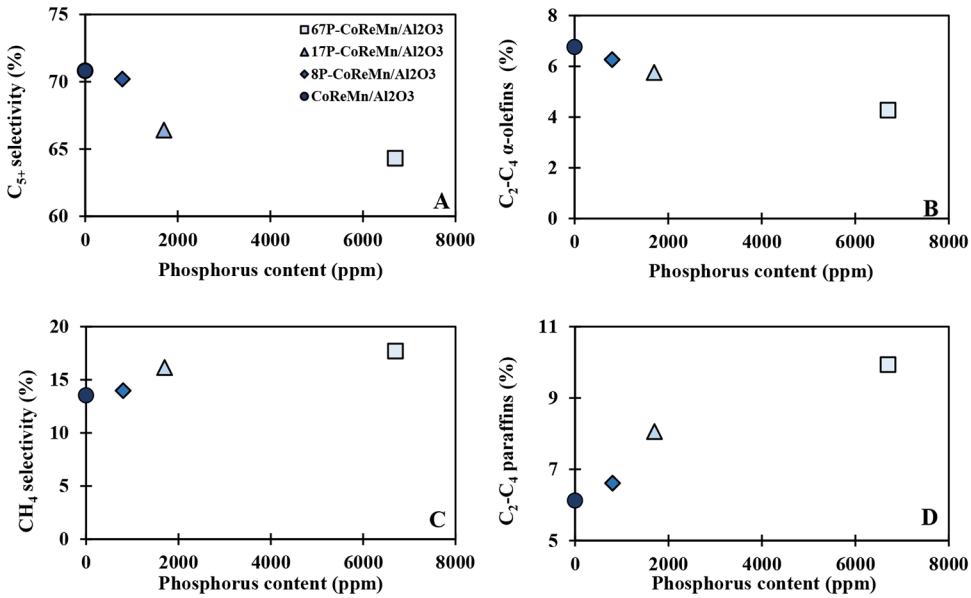

Fig. 5 Selectivity towards C_{5+} (A), C_2-C_4 alpha-olefins (B), methane (C) and C_2-C_4 paraffins (D) of $CoReMn/Al_2O_3$ with increasing phosphorus loading. The selectivity measures were carried out after the first 24 h on stream, at 240 ºC, 5 bar and different space velocities to achieve 50% CO conversion

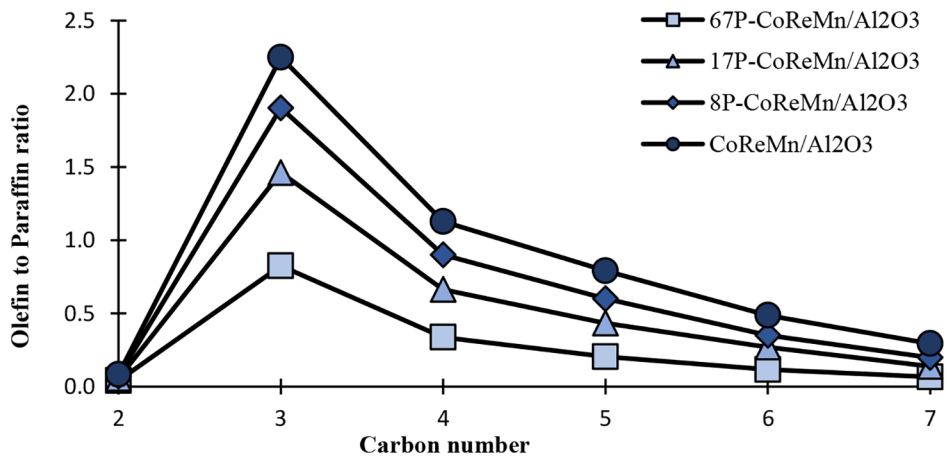

Fig. 6 Olefin to paraffin ratio depending on the carbon number, from 2 to 7, of $CoReMn/Al_2O_3$ with increasing phosphorus loading

Figure 6 shows the olefin to paraffin (O/P) ratio based on the carbon number for the different catalysts. The ratio decreases as the carbon number increases with propene being the largest fraction of the light olefin products. As expected, the O/P ratio decreases with the addition of phosphorus due to the increase in the hydrogenation products [35].

The effect of phosphorus on the selectivity cannot be explained by the hydrogen desorption as there were no differences in the H_2-TPD between the reference and the poisoned catalysts. Consequently, a different reaction mechanism or electronic effects due to the phosphorus addition might be the cause of this increase in hydrogenation activity, as also mentioned in the activity measurement section. Previous studies [36] showed that the addition of phosphorus leads to a decrease in C_{5+}. However, this effect was not explained in the analysis. In the same work, they studied the effect of alkali metals on the cobalt catalyst and the result showed an opposite effect on the selectivity, with an increased C_{5+} production and lower methane and short chain olefins selectivity. It is explained that the electronegativity of the promoters and supports can play a role in the electronic density of the cobalt catalyst. Equally, as supported by Tatsumi et al. [32], the CO-metal bond strongly depends on the electron back-donation from the metal to CO, therefore electronegative oxides, as phosphorus oxide, decreases the electron density due to electron withdrawal and therefore, it weakens the bond between the metal and the CO. This reduction in the CO bond energy could imply that CO is adsorbed weaker on the cobalt particles and this in turn influences the H/CO ratio on the catalyst surface, favoring chain termination by hydrogenation. This increased effective surface H/CO ratio, as explained before, might also contribute to the decrease in the catalyst activity due to the weakened CO bond energy.

4 Conclusion

The effect of different loading of phosphorus has been investigated in a cobalt-based catalyst. The activity of the catalysts decreased with increased loading of phosphorus. However, this decrease did not appear to be linear with the amount of poison. These results showed that there is a threshold amount, somewhere above 800 ppm, where the phosphorus loading starts to affect the catalytic activity. This limit was also visible in the reducibility of the catalyst and the metallic dispersion, with a reduction with increased content loading. At the same time, the effect on the selectivity is noticeable also at the lowest loading as seen from an increase in hydrogenated products as methane and paraffins and a reduced chain growth probability. This knowledge can be translated to requirements for cleaning the syngas, which in turn can lead to more economic and more viable BTL process.

Acknowledgements We are grateful to The Norwegian Research council for funding through contract nº 257622.

Funding Open access funding provided by NTNU Norwegian University of Science and Technology (incl St. Olavs Hospital - Trondheim University Hospital)

Open Access This article is licensed under a Creative Commons Attribution 4.0 International License, which permits use, sharing, adaptation, distribution and reproduction in any medium or format, as long as you give appropriate credit to the original author(s) and the source, provide a link to the Creative Commons licence, and indicate if changes were made. The images or other third party material in this article are included in the article's Creative Commons licence, unless indicated otherwise in a credit line to the material. If material is not included in the article's Creative Commons licence and your intended use is not permitted by statutory regulation or exceeds the permitted use, you will need to obtain permission directly from the copyright holder. To view a copy of this licence, visit http://creativecommons.org/licenses/by/4.0/.

References

1. Net Zero by 2050 - A Roadmap for the Global Energy Sector (2022) International Energy Agency, https://www.iea.org/reports/net-zero-by-2050, Accessed 29
2. Amghizar I, Vandewalle LA, van Geem KM, Marin GB(2017) New Trends in Olefin Production, Engineering, 3:171–178
3. Marsh M(2019) J Wery Filling the propylene gap. Shaping the future with on-purpose technologies, Honeywell UOP, https://www.hydrocarbonengineering.com/whitepapers/honeywell-uop/, Accessed 30 Aug. 2022
4. Torres Galvis HM, de Jong KP (2013) Catalysts for production of lower olefins from synthesis gas: a review. ACS Catal 3:2130–2149
5. Dement'Ev KI, Sagaradze AD, Kuznetsov PS, Palankoev TA, Maximov AL (2020) Selective production of light olefins from Fischer-Tropsch Synthetic Oil by Catalytic cracking. Ind Eng Chem Res 59:15875–15883
6. Liu Y, Kamata H, Ohara H, Izumi Y, Ong D, Chang J, Poh C, Chen L, Borgna A (2020) Low-olefin production process based on Fischer-Tropsch synthesis: process synthesis, optimization, and Techno-Economic Analysis. Ind Eng Chem Res 59:8728–8739
7. Hilmen AM, Schanke D, Holmen A (1996) TPR study of the mechanism of rhenium promotion of alumina-supported cobalt Fischer-Tropsch catalysts. Catal Lett 38:143–147
8. Pedersen E, Svenum IH, Blekkan EA (2018) Mn promoted Co catalysts for Fischer-Tropsch production of light olefins – an experimental and theoretical study. J Catal 361:23–32
9. Morales F, Grandjean D, Mens A, de Groot FMF, Weckhuysen BM (2006) X-ray absorption spectroscopy of Mn/Co/TiO_2 Fischer-Tropsch catalysts: Relationships between preparation method, molecular structure, and catalyst performance. J Phys Chem B 110:8626–8639
10. Fishery and aquaculture statics Food and Agriculture Organization of the United Nations, Statistics FAO(2019) www.fao.org/fishery/static/Yearbook/YB2019_USBcard/index.htm, Accessed 29 Aug. 2022
11. Freitas SR, Soria JA (2011) Development of a gasification system for utilizing fish processing waste and coastal small diameter wood in rural areas. Energy Fuels 25:2292–2300
12. Rowland S, Bower CK, Patil KN, DeWitt CAM(2009) Updraft gasification of salmon processing waste, *Journal of Food Science*, 74 – 8: 426–431
13. Rauch R, Hrbek J, Hofbauer H(2014) Biomass gasification for synthesis gas production and applications of the syngas', Wiley Interdisciplinary Reviews: Energy and Environment, 3:343–362
14. Dimitriou I, Goldingay H, Bridgwater Av (2018) Techno-economic and uncertainty analysis of Biomass to Liquid (BTL) systems for transport fuel production. Renew Sustain Energy Rev 88:160–175
15. Couto N, Rouboa A, Silva V, Monteiro E, Bouziane K (2013) Influence of the biomass gasification processes on the final composition of syngas. Energy Procedia 36:596–606
16. Frandsen F, Dam-Johansen K, Rasmussen P (1994) Trace elements from combustion and gasification of coal- An equilibrium approach. Prog Energy Combust Sci 20:115–138
17. Vassilev S, Baxter D, Andersen L, Vassileva C (2010) An overview of the chemical composition of biomass. Fuel 89:913–933
18. Masiá AT, Buhre BJP, Gupta RP, Wall TF (2007) Characterising ash of biomass and waste. Fuel Process Technol 88:1071–1081
19. Turnan SC, Kinoshitaa CM, Lshimuraa DM, Zhoub J (1998) The fate of inorganic constituents of biomass in fluidized bed gasification. Fuel 77:135–146
20. Gnanamani MK, Jacobs G, Pendyala V, Graham M, Hopps S, Thomas G, Shafer W, Sparks D, Xiao Q, Hu Y (2016) Fischer-Tropsch synthesis: anchoring of cobalt particles in phosphorus modified cobalt/silica catalysts. Appl Catalysis: Gen 523:146–158
21. Martinelli M, Kumaran Gnanamani M, Hopps S, Sparks D, MacLennan A, Hu Y, Davis BH, Jacobs G (2018) Effect of Phosphorus on the Activity and Stability of Supported Cobalt Catalysts for Fischer-Tropsch Synthesis, ChemCatChem, 10: 3709–3716
22. Park SJ, Bae JW, Jung G, Ha K, Jun K, Lee Y, Park H (2012) Crucial factors for catalyst aggregation and deactivation on Co/Al_2O_3 in a slurry-phase Fischer-Tropsch synthesis, vol 413–414. A General, Applied Catalysis, pp 310–321
23. il Ahn C, Park YM, Cho JM, Lee DH, Chung C, Cho BG, Bae JW (2016) Fischer-Trospch synthesis on ordered Mesoporous Cobalt-Based catalysts with Compact Multichannel Fixed-Bed Reactor Application: a review. Catal Surv Asia 20:4:210–230
24. Park SJ, Cho JM, Ahn C, Lee Y, Jun K, Cho BG, Bae JW (2017) Roles of phosphorous-modified Al2O3 for an enhanced stability of Co/Al2O3 for CO hydrogenation to hydrocarbons. J Mol Catal A: Chem 426:177–189

25. Pedersen E, Blekkan EA (2018) Noble Metal Promoted CoMn Catalysts for Fischer–Tropsch Synthesis. Catal Lett 148:1027–1034
26. Schanke D, Vada S, Blekkan EA, Hilmen AM, Hoff A, Holmen A (1995) Study of Pt-promoted Cobalt CO Hydrogenation catalysts. J Catal 156:85–95
27. Jones RD, Bartholomew CH (1998) Improved Flow technique for measurement of Hydrogen Chemisorption on Metal catalysts. Appl Catal 39:77–88
28. Bezemer G, Bitter J, Kuipers H, Oosterbeek H, Holewijn J, Xu X, Kapteijn F, Jos A, van Dillen(2006) and K. P. de Jong., Cobalt particle size effects in the Fischer-Tropsch reaction studied with carbon nanofiber supported catalysts, Journal of the American Chemical Society, 128:3956–3964
29. Bradford MCJ, Te M, Pollack A(2005) Monolith loop catalytic membrane reactor for Fischer-Tropsch synthesis, Applied Catalysis: A General, 283: 39–46
30. Stobbe ER, de Boer BA, Geus JW (1999) The reduction and oxidation behavior of manganese oxides. Catal Today 47:1–4
31. Iglesia E (1997) Review Design, synthesis, and use of cobalt-based Fischer-Tropsch synthesis catalysts. Appl Catalysis: Gen 161:59–78
32. Ishihara T, Eguchi K, Arai H (1992) Importance of surface hydrogen concentration in enhancing activity of co-ni alloy catalyst for CO hydrogenation. J Mol Catal 72:253–261
33. Iqbal S, Davies T, Morgan J, Karim K, Bartley J, Taylor S, Hutchings G (2016) Fischer Tropsch synthesis using promoted cobalt-based catalysts. Catal Today 272:74–79
34. Iglesia E, Reyes SC, Madon RJ (1991) Transport-enhanced a-Olefin readsorption pathways in Ru-Catalyzed Hydrocarbon Synthesis. J Catal 129:238–256
35. Borg Ø, Dietzel P, Spjelkavik A, Tveten E, Walmsley J, Diplas S, Eri S, Holmen A, Rytter E (2008) Fischer-Tropsch synthesis: cobalt particle size and support effects on intrinsic activity and product distribution. J Catal 259:161–164
36. Borg Ø, Hammer N, Enger B, Myrstad R, Lindvg O, Eri S, Skagseth T, Rytter E (2011) Effect of biomass-derived synthesis gas impurity elements on cobalt Fischer-Tropsch catalyst performance including in situ sulfur and nitrogen addition. J Catal 279:163–173

Publisher's Note Springer Nature remains neutral with regard to jurisdictional claims in published maps and institutional affiliations.